

# Signal-to-Noise Ratio and Parallel Imaging Performance of a 16-Channel Receive-Only Brain Coil Array at 3.0 Tesla

Jacco A. de Zwart,<sup>1\*</sup> Patrick J. Ledden,<sup>2</sup> Peter van Gelderen,<sup>1</sup> Jerzy Bodurka,<sup>3</sup> Renxin Chu,<sup>1</sup> and Jeff H. Duyn<sup>1</sup>

**The performance of a 16-channel receive-only RF coil for brain imaging at 3.0 Tesla was investigated using a custom-built 16-channel receiver. Both the image signal-to-noise ratio (SNR) and the noise amplification (*g*-factor) in sensitivity-encoding (SENSE) parallel imaging applications were quantitatively evaluated. Furthermore, the performance was compared with that of hypothetical coils with one, two, four, and eight elements (*n*) by combining channels in software during image reconstruction. As expected, both the *g*-factor and SNR improved substantially with *n*. Compared to an equivalent (simulated) single-element coil, the 16-channel coil showed a 1.87-fold average increase in brain SNR. This was mainly due to an increase in SNR in the peripheral brain (an up to threefold SNR increase), whereas the SNR increase in the center of the brain was 4%. The incremental SNR gains became relatively small at large *n*, with a 9% gain observed when *n* was increased from 8 to 16. Compared to the (larger) product birdcage head coil, SNR increased by close to a factor of 2 in the center, and by up to a factor of 6 in the periphery of the brain. For low SENSE acceleration (rate-2), *g*-factors leveled off for *n* > 4, and improved only slightly (1.4% averaged over brain) going from *n* = 8 to *n* = 16. Improvements in *g* for *n* > 8 were larger for higher acceleration rates, with the improvement for rate-3 averaging 12.0%. Magn Reson Med 51:22–26, 2004. Published 2003 Wiley-Liss, Inc.†**

**Key words:** RF coil array; parallel imaging; MR Hardware; RF coil design; SNR

The sensitivity of MRI is dependent on the type of radio-frequency (RF) coil used for signal reception. Although birdcage-type volume coils (1) have been used extensively for brain imaging, their sensitivity is inferior to that of array coils (2). For properly designed arrays, this is true not only in regions close to the coils, but also at any position in the object (3).

The recent increase in applications of parallel imaging techniques (4,5) has led to renewed interest in the design of MRI RF coils. In turn, the number of receive channels in commercial MRI scanners is poised to grow over the next few years. This might lead to a widespread use of array

coils for both parallel imaging and improved sensitivity in conventional imaging.

Results from simulations and experiments suggest that with the use of coil arrays that fully cover the object surface, and when sample noise is the dominant noise source, the image signal-to-noise ratio (SNR) increases with the number of coil elements (2,3). This is true for regions in the object that are close to the coil array, and to a lesser extent also for the SNR averaged over the object. The SNR in the center of the array does not change substantially with the number of coil elements.

However, in arrays with an increasing number of smaller coils, noise sources other than sample noise (e.g., resistive coil noise and/or preamplifier noise) can contribute substantially to the overall noise, and eventually SNR gains level off and turn into losses. Since sample noise increases more rapidly with field strength than do the other noise sources, optimized arrays at high field will have smaller coils and thus a larger number of elements.

For parallel imaging performance, both SNR and the spatial interaction between the sensitivity profiles of the individual coils are important. The latter can be quantified by the so-called *g*-factor (5), and generally improves with the number of coil elements used. Coils with improved (lower, closer to 1) *g*-factors allow parallel imaging with higher acceleration rates while they minimize noise amplification.

Factors that govern the ultimately achievable coil performance include the inherent electromagnetic wave properties of the sample, as well as practical aspects such as coil resistivity, losses in the electronic components of the coil and preamplifier, and inductive coupling between coil elements. These practical issues determine how small the elements can be made, and how many elements are contained in the array. For imaging of the human brain, a practical eight-channel coil can be built with excellent SNR and parallel imaging performance (3,6). Minimal inductive coupling can be achieved by the use of low-impedance preamplifiers and positioning the elements close to the brain (3).

To investigate the feasibility of improving performance by increasing the number of coil elements, we designed and built a 16-channel brain coil for operation at 3.0 T. To allow quantitative evaluation of coil performance as a function of the number of coil elements, simulated data for a number of array configurations were synthesized from the 16-channel coil data by combining channels in software. For reference, the coil SNR was also compared to that of the standard birdcage head coil.

<sup>1</sup>Advanced MRI Section, Laboratory of Functional and Molecular Imaging, NINDS, National Institutes of Health, Bethesda, Maryland.

<sup>2</sup>Nova Medical Inc., Wakefield, Massachusetts.

<sup>3</sup>Functional MRI Facility, NIMH, National Institutes of Health, Bethesda, Maryland.

\*Correspondence to: Jacco de Zwart, AMRI/LFMI/NINDS, National Institutes of Health, 10 Center Dr., Bldg. 10, Rm. B1D-118, Bethesda, MD 20892-1065. E-mail: Jacco.deZwart@nih.gov

Received 16 June 2003; revised 12 August 2003; accepted 28 August 2003. DOI 10.1002/mrm.10678

Published online in Wiley InterScience (www.interscience.wiley.com).

Published 2003 Wiley-Liss, Inc. † This article is a US Government work and, as such, is in the public domain in the United States of America.

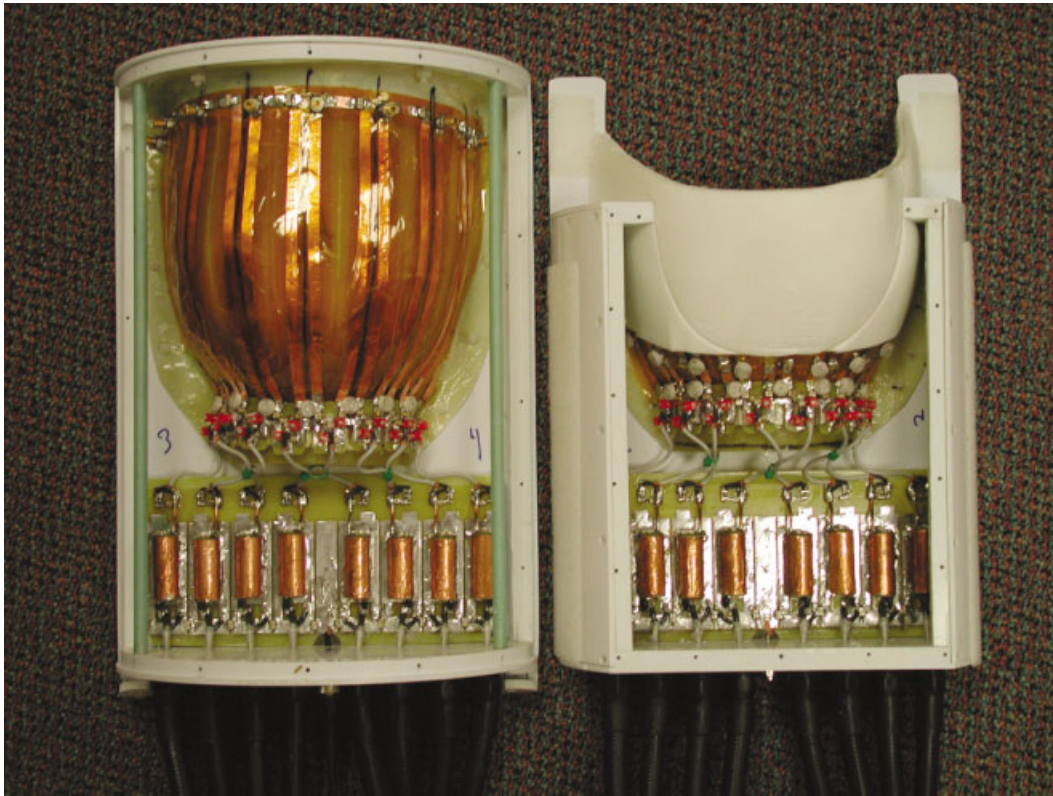


FIG. 1. Layout of the individual coil elements in both the top (right) and bottom (left) halves of the 16-channel coil. Note that the actual coil elements in the top half are mostly covered by white protective foam. The copper conductors of the coil elements in the bottom half are visible through the yellow kapton insulating material. See text and Refs. 8 and 10 for more details.

## MATERIALS AND METHODS

The experiments were performed on a 3.0 T GE Signa VH/3 (90-cm bore, whole-body transmit/receive coil) with advanced control gradient driver (ACGD) gradients ( $40 \text{ mT}\cdot\text{m}^{-1}$ ,  $150 \text{ T}\cdot\text{m}^{-1}\cdot\text{s}^{-1}$ ). All experiments were performed with an echo-planar imaging (EPI) sequence that was developed in-house. This sequence features ramp sampling (data were acquired on 50% of the ramps) and can be run in either gradient-echo or spin-echo mode.

The experiments were performed on consenting, normal volunteers in accordance with an NIH-approved protocol (IRB approval number 00-N-0082, last reviewed on January 22, 2003).

Unless stated otherwise, the experiments were performed using a custom-built 16-channel coil array (model NMSC025-3T; Nova Medical Inc., Wakefield, MA), as depicted in Fig. 1. The coil elements were placed around the head in a single row (the design is similar to a previously described eight-element design (3)). To achieve whole-brain coverage and at the same time maximize the visual field of the volunteer, the posterior coil elements were longer than the anterior elements. The 16 curved trapezoidal elements were laid out with 6.25-mm-wide copper tape on a two-piece fiberglass former (see Fig. 1). The elements were about 2.0 cm wide and separated by a 0.7-cm gap, resulting in a gap-to-element ratio of 0.3. They were tuned to 127.8 MHz with multiple distributed capacitors, and matched to a 50  $\Omega$  coaxial cable by means of a

lumped-element bridge balun circuit. The coils were actively detuned during transmit using a PIN-diode across the cable side of the balun. In addition, passive detuning traps were included on each element. Inductive coupling between adjacent elements on the top and bottom formers was minimized by capacitive isolating circuits (7).

Each element was connected to an ultra-low-impedance preamplifier (8) with  $<1 \Omega$  input impedance and 35 dB of gain at 127.8 MHz (model NMP-002A; Nova Medical Inc., Wakefield, MA). Isolation between all channels was  $>20$  dB. The preamplifiers were connected to an in-house-built 16-channel receiver (9,10). To enable a proper comparison with array coil data, the head coil data were also acquired using one channel of the 16-channel receiver.

For the SNR performance evaluation, the following scan parameters were used: 4000-ms repetition time (TR); 50-ms echo time (TE); 26 3.5-mm-thick oblique-axial slices; 0.5-mm interslice gap;  $220 \times 165 \text{ mm}^2$  field of view (FOV);  $128 \times 96$  matrix size, leading to a nominal voxel size of  $1.7 \times 1.7 \times 3.5 \text{ mm}^3$ ; 71.4-ms acquisition window duration; 50% ramp sampling; 500-kHz bandwidth; two-fold oversampling; and  $90^\circ$  flip angle. High-resolution rate-2 SENSE EPI data were acquired with a matrix size of  $192 \times 144$  (nominal voxel size of  $1.1 \times 1.1 \times 3.5 \text{ mm}^3$ ), a 72.3-ms acquisition train length, and otherwise identical settings. The readout gradient was applied in the anterior-posterior direction.

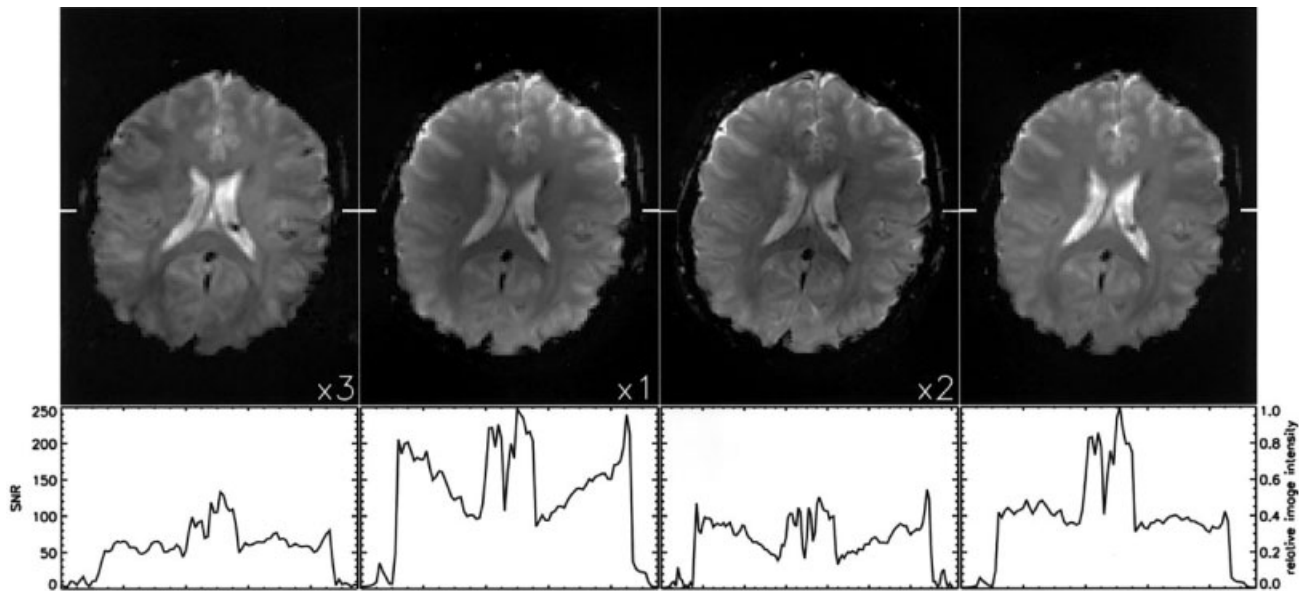


FIG. 2. Performance of the 16-channel coil compared to the standard 28-cm GE birdcage head coil. The top row shows a single slice of the acquired EPI data. The three leftmost images are SNR maps. Their relative scaling factor is indicated in the lower right corner of the image. The rightmost image shows the same data as in the second image, after intensity correction. Tick marks left and right in each image indicate the location of the profile shown below it. The first column shows single-shot EPI data from the birdcage head coil ( $128 \times 96$  resolution). Data in all other columns were acquired with the 16-channel coil. Data in the second and third columns were acquired at respectively the same ( $128 \times 96$ ) and higher ( $192 \times 144$ , rate-2 SENSE) spatial resolution. Note that the scaling of the rightmost column is arbitrary. See text for more details.

SENSE data were reconstructed with methods similar to those described previously (5,11), using coil sensitivity maps derived from the data (11). A small modification was made to the calculation of relative coil sensitivities. This involved the generation of a sensitivity reference map by addition of the individual coil images with constant phase (derived from a  $4 \times 4$  region in the center of an image). The resulting sensitivity reference map (and reconstructed SENSE images) showed a relatively uniform intensity distribution. To derive image SNR, the reconstructed SENSE images were divided by the square root of the covariance computed in the SENSE reconstruction (11). The SNR of the birdcage coil data was computed by dividing the magnitude image data by the average of the standard deviation (SD) in the real and imaginary parts of the noise data. In order to obtain noise data, the EPI sequence does not execute the RF excitation during the first volume of the time series. In a SENSE experiment, such a noise volume is used to compute the noise correlation matrix.

The 16-channel coil data that were acquired with a  $128 \times 96$  matrix size were also used to evaluate SNR and SENSE performance as a function of the number of coil elements. Sixteen of the slices, covering the brain from the very top down to a plane through the lower parts of the frontal lobes and the middle of the cerebellum, were used. To simulate data acquired with less than 16 coil elements, complex data from neighboring coil elements were combined in software. To synthesized data representing 8-, 4-, and 2-channel coils were obtained by combining data from groups of 2, 4, and 8 neighboring channels, respectively. A birdcage coil was synthesized by combining all 16 channels into one. Electromagnetic simulations indi-

cated that the performance of these synthetic coils derived by combining channels was similar (to within 5%) to that of actual coils (data not shown). In order to combine channels, image data were summed after the phase was equalized in the center of the coil. The center phase was derived from a 4-by-4-pixel rectangle in the center of each image (see above). All possible combinations of neighboring coil elements were evaluated (e.g., for simulated eight-element coil data, there are two possible combinations of neighboring elements: [1+2, 3+4, . . . , 15+16] and [2+3, 4+5, . . . , 16+1]; a simulated four-element coil has four possible combinations, and a two-element coil has eight possible combinations).

The data were trimmed to a  $96 \times 96$  matrix size to narrowly encompass the head at its largest diameter. The SNR and  $g$ -factor were averaged over the entire brain (a mask was derived by thresholding an intensity-weighted image). Undersampling was simulated in either the read-out or phase-encode direction (1D-SENSE), or both (2D-SENSE). Undersampling of data in the slice-select dimension, as described recently (12), was not investigated in this study.

## RESULTS AND DISCUSSION

Figure 2 shows the SNR performance of the 16-channel coil compared to that of the standard GE 28-cm-diameter birdcage head coil. SNR-scaled data acquired at the identical resolution (first and second columns) show an SNR improvement in excess of a factor of 4 in the periphery, and an approximately twofold SNR increase in the center of the brain. Rate-2 SENSE data, acquired at a 2.25-fold-

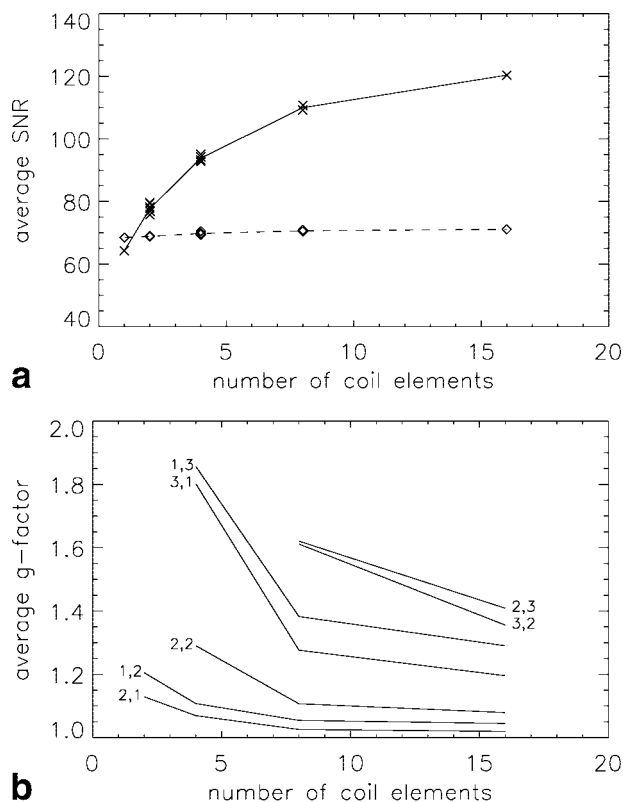


FIG. 3. **a**: Image SNR as a function of the number of coil elements averaged over the whole brain (solid line) or the center of the brain (broken line). Symbols show the SNR for each of the possible simulated coil configurations for the whole brain ( $\times$ ) and the center of the brain ( $\diamond$ ). **b**: The average SENSE  $g$ -factor in the brain as a function of the SENSE acceleration rate in the readout ( $r$ ) and phase-encode ( $p$ ) directions, and the number of coil elements. The values next to each line indicate the SENSE acceleration factor as  $r,p$ . See text for more details.

reduced nominal voxel volume (Fig. 2, third column) show a similar SNR in the center of the brain and a close to twofold SNR increase in the brain periphery when compared to the birdcage data at a larger voxel volume. For reference, an intensity-corrected image (obtained using the fixed phase addition of coil data to obtain a sensitivity reference) is also shown (Fig. 2, right column). The intensity distribution of these data more closely resembles that of the birdcage coil (left column).

Figure 3a shows the average image SNR in the brain as a function of the number of coil elements (solid line). The dashed line shows similar data for the center of the brain (approximately in the mediodorsal thalamic nuclei), in a region of interest (ROI) comprised of 154 voxels. Wherever coils could be combined in multiple ways (in the case of two, four, or eight coils (see Materials and Methods section)), the spatially averaged SNR for all possible cases is indicated ( $\times$  and  $\diamond$ ). The plot lines run through the average of those data. The average image SNR increases by a factor of 1.21, 1.46, 1.71, and 1.87 when going from 1 to 2, 4, 8, and 16 elements, respectively. As expected from simulations (3), signals from the small ROI in the center of the brain show virtually no SNR increase as a function of

the number of coil elements (SNR increased 4% for 16 independent channels compared to a single channel).

Figure 3b shows the average  $g$ -factor in the brain for various SENSE acceleration rates as a function of the number of coil elements. Whenever neighboring coils could be combined in multiple ways, the coil-combination leading to the lowest average  $g$ -value was used. Maps of the  $g$ -factor for both 1D and 2D SENSE were computed. The label  $r,p$  next to a curve indicates the SENSE acceleration factor in the readout and phase-encode directions, respectively (e.g., the label 1,2 indicates rate-2 SENSE in the phase-encode direction, the rate-2 SENSE mode originally described by Pruessman et al. (5)). The data show that the increase in SENSE performance when going from 8 to 16 channels is limited for rate-2-based SENSE (0.6%, 0.9%, and 2.6% for rate-2,1, rate-1,2, and rate-2,2, respectively). However, the use of 16 channels vs. 8 channels is significantly more beneficial for rate-3-based SENSE methods, where performance increases by 6.7%, 7.2%, 18.9%, and 15.0% for rate-3,1, 1,3, 3,2, and 2,3, respectively.

These results indicate that although the increase in average image SNR levels off with an increasing number of coil elements, substantial improvements in higher-rate parallel imaging performance are achieved when the number of coil elements is augmented from 8 to 16. With a 16-element coil in this specific configuration, the reconstruction-related SNR penalty for using rate-3 SENSE is still on the order of 20–30%, which potentially can be largely overcome with an increased number of coil elements. For brain MRI at magnetic field strengths of 3.0 T (and above), coils can still be reduced by at least a factor of 2 in size before the system is no longer dominated by sample noise (3). Such systems would therefore benefit from coil arrays with more than 16 coil elements, especially for parallel imaging applications.

Results have shown that rate-2,2 SENSE leads to a lower average  $g$ -factor than both rate-3,1 and rate-1,3 SENSE. For 16 coil elements, the noise amplification averages  $<10\%$  for rate-2,2, compared to 20–30% for the two versions of rate-3. At the same time, this mode results in a higher imaging acceleration factor (fourfold compared to threefold).

Note that the experiments described here involve a significantly increased amount of more acquired data compared to a typical fMRI experiment using the birdcage head coil. In order to reconstruct the data in a time frame similar to that in which they were acquired, the data were processed in parallel on 12 computers with dual 2.2 GHz Intel Xeon CPUs (10). This \$30000 array of computers enabled us to reconstruct a typical 10-min fMRI experiment ( $192 \times 144$  image matrix size, 10 slices, 1000-ms TR, twofold oversampling, rate-2 SENSE, 50% ramp sampling) in approximately 15 min. The size of the raw data was approximately 12 GB.

## CONCLUSIONS

We have shown that the use of a 16-channel array coil for MRI of the human brain is technically and practically feasible, and allows for a substantial SNR increase in parallel imaging applications. The possibility of further in-

creasing the number of coil channels and applying this technology to MRI at 7.0 T is currently being investigated.

## ACKNOWLEDGMENTS

The authors thank Susan O'Flahavan (LFMI/NINDS/NIH) for her assistance with the experiments, and Peter Kellman (LCE/NHLBI/NIH) and Alan Koretsky (LFMI/NINDS/NIH) for helpful discussions.

## REFERENCES

1. Hayes CE, Axel L. An efficient, highly homogeneous radiofrequency coil for whole-body NMR imaging at 1.5 T. *J Magn Reson* 1985;63:622–628.
2. Roemer PB, Edelstein WA, Hayes CE, Souza SP, Mueller OM. The NMR phased array. *Magn Reson Med* 1990;16:192–225.
3. de Zwart JA, Ledden PJ, Kellman P, van Gelderen P, Duyn JH. Design of a SENSE-optimized high-sensitivity MRI receive coil for brain imaging. *Magn Reson Med* 2002;47:1218–1227.
4. Sodickson DK, Manning WJ. Simultaneous acquisition of spatial harmonics (SMASH): fast imaging with radiofrequency coil arrays. *Magn Reson Med* 1997;38:591–603.
5. Pruessmann KP, Weiger M, Scheidegger MB, Boesinger P. SENSE: sensitivity encoding for fast MRI. *Magn Reson Med* 1999;42:952–962.
6. King SB, Duensing GR, Peterson D, Varosi S, Molyneaux DA. A comparison of 1, 4 and 8 channel phased array head coils at 1.5T. In: Proceedings of the 9th Annual Meeting of ISMRM, Glasgow, Scotland, 2001. p 1090.
7. Ledden P, de Zwart J, van Gelderen P, Bodurka J, Duyn J. Sixteen channel gapped SENSE array for brain imaging at 3T. In: Proceedings of the 11th Annual Meeting of ISMRM, Toronto, Canada, 2003. p 466.
8. Ledden PJ, Inati S. Four channel preamplifier decoupled phased array for brain imaging at 1.5T. In: Proceedings of the 9th Annual Meeting ISMRM, Glasgow, Scotland, 2001. p 1117.
9. Chu R, Bodurka J, Ledden P, van Gelderen P, Kellman P, Morris D, de Zwart JA, Duyn JH. A scaleable multi-channel MR data acquisition system. In: Proceedings of the 11th Annual Meeting of ISMRM, Toronto, Canada, 2003. p 711.
10. Bodurka J, Ledden P, van Gelderen P, Chu R, de Zwart JA, Morris D, Duyn JH. Scaleable multi-channel MRI data acquisition system. *Magn Reson Med*, 2004;51:165–171.
11. de Zwart JA, van Gelderen P, Kellman P, Duyn JH. Application of sensitivity-encoded echo-planar imaging for blood oxygen level-dependent functional brain imaging. *Magn Reson Med* 2002;48:1011–1020.
12. Larkman DJ, Hajnal JV, Herlihy AH, Coutts GA, Young IR, Ehnholm G. Use of multicoil arrays for separation of signal from multiple slices simultaneously excited. *J Magn Reson Imaging* 2001;13:313–317.